ISSN 1541-308X, Physics of Wave Phenomena, 2015, Vol. 23, No. 4, pp. 279–291. © Allerton Press, Inc., 2015.

REMOTE SENSING OF NATURAL MEDIA

Interference and Phase Structure of the Low-Frequency Vector-Scalar Field in Shallow Water for Variable Reception or Transmission Depths

G. N. Kuznetsov[1]* and A. N. Stepanov[2]**

[1] *Wave Research Center, Prokhorov General Physics Institute, Russian Academy of Sciences, ul. Vavilova 38, Moscow, 119991 Russia*

[2] *Samara State University, ul. Akad. Pavlova 1, Samara, 443011 Russia*

Received August 10, 2015

Abstract—Relations for calculating the amplitude and phase characteristics of sound pressure and orthogonal projections of the vibration velocity vector and phase gradient in shallow water have been derived. Dependences of the effective phase velocity of equivalent plane wave, orthogonal projections of the gradient of sound pressure phase, and projections of the vibration velocity vector on the transmitter (or receiver) depth are calculated for different frequencies and location depths of receivers (and transmitters). It is found that the horizontal projections of the vibration velocity vector and phase gradient satisfy the reciprocity principle whereas their vertical projections do not obey this principle. Therefore, the characteristics of the vertical components must be studied independently with variation in their transmission or reception depth. It is shown that, for low frequencies and variable transmitter or receiver depth, the effective phase velocities in interference maxima exceed generally the speed of sound in water by 5–15% or even more. Some recommendations on the use of sound field characteristics in the regions of maximum sound pressure for solving problems of direction finding and signal detection are formulated. The behavior of the characteristics of arrival angles of equivalent plane wave with variation in the transmission or reception depth are investigated.

DOI: 10.3103/S1541308X15040068

1. INTRODUCTION

There are three typical classes of problems in applied hydroacoustics:

(i) reception of signals from a source located at unknown depth is performed by a horizontal antenna placed on a specified horizon; in this case, one must investigate the field parameters with variation in the source depth (from the bottom to the free surface) to determine the characteristics of the receiving antenna response.

(ii) transmission is implemented in a waveguide by vertical (blocking the waveguide) antennas, the field of signals of which is received at specified depths;

(iii) transmission is carried out at a specified depth, and reception is performed using a vertical (blocking the waveguide) antenna.

Sound sources (single or vertically spaced) can play the role of transmitters. Extended multi-element horizontal or vertical antennas, composed of scalar or multicomponent vector-scalar receivers, can be used as receiving antennas.

The amplitude-phase structure of the field on the aperture of these antennas has been investigated (see, for example, [1–5]). It was established that, in contrast to free space, where waves propagate retaining the in-phase condition for the sound pressure and vibration velocity, and the plane-wave propagation direction always coincides with the sound pressure (SP) phase gradient, a difficult-to-predict interference field structure (determined by various factors) is formed in a real waveguide. The in-phase condition for the SP and different projections of vibration velocity vector (VVV) in this field is violated. Generally, the directions of the VVV and SP phase gradient do not coincide.

2. APPROXIMATING MODEL OF LOW-FREQUENCY FIELD IN SHALLOW WATER

Let us consider the opportunity of approximate description of the amplitude-phase field structure using

*E-mail: skbmortex@mail.ru

**E-mail: stepanovanni@gmail.ru

simple approximating dependences. Such an attempt was made in [3] to describe the phase gradients for the regions of interference maxima ($P_{\max}$). It was found that the dependence of the SP phase φ on distance and grad φ in these regions can approximately be described by means of the approximating dependence of the effective phase velocity,

$$C_{\varphi}^{*} = \sum_{l=1} C_{\varphi l} W_l^2 \Big/ \sum_{l=1} W_l^2, \qquad (1)$$

where $C_{\varphi l}$ is the phase velocity of the lth normal wave and W_l is its amplitude. The corresponding relation for the effective (weighted average) group velocity has the form

$$C_{\mathrm{g}}^{*} = \sum_{l=1} C_{\mathrm{g}l} W_l^2 \Big/ \sum_{l=1} W_l^2, \qquad (2)$$

where $C_{\mathrm{g}l}$ is the group velocity of the lth normal wave. It is assumed that, using the expressions for C_{φ}^{*} in the $P_{\max}$ regions, one can approximately calculate the phase shifts for tone signals in spaced points, and, using the C_{g}^{*} values, one can estimate the group delay times for pulse signals. Obviously, C_{φ}^{*} and C_{g}^{*} are $C_{\varphi,\mathrm{g}}^{*}(r,\omega,h,z,z_0)$ and $C_{\varphi}^{*}\times C_{\mathrm{g}}^{*} \approx C_0^2$, where C_0 is the speed of sound in water. Hereinafter, r is the distance between the transmitter and receivers; $\omega = 2\pi f$ is the circular frequency; h is the waveguide depth; z and z_0 are, respectively, the receivers' and transmitter location depths; and f is the acoustic signal frequency. It is also assumed that C_{φ}^{*} and C_{g}^{*} are the phase and group velocities of equivalent plane wave (EPW), approximating with a certain accuracy the real field in $P_{\max}$ regions.

Then we analyze the specific features of the C_{φ}^{*} quantity, which can be used to form desired directional characteristics of antenna.

These problems were analyzed numerically in [4] for different hydrophysical conditions of sound propagation through a waveguide. It was shown that, with an increase in distance, C_{φ}^{*} tends to a constant value; however, it exhibits a natural dependence on the soil hardness and sound frequency. It was found in [5] that, using the C_{φ}^{*} value (C^{*} below) instead of the speed of sound in water (C_0) and processing the signal at the frequencies for which the antenna is located in the $P_{\max}$ region, the directional characteristic of the antenna yields unbiased estimates of the the bearing γ, and the lateral field does not contain any spikes. On the contrary, when the antenna aperture is located in the region of interference minimum of the field ($P_{\min}$), the directional characteristic is split, the bearing estimates are biased, and the lateral field increases. The estimate bias for bearing γ obtained with C_0 instead of C^{*} appears to be natural because the C_0 value is inconsistent with the real SP phase gradient on the antenna aperture.

An approximate estimate of C^{*} can be obtained using relation (1), which takes into account all modes propagating in the waveguide or only groups of the most coherent modes with close wavenumbers. Dependences $C^{*}(r,\omega,h,z,z_0)$ can also be determined numerically within, e.g., the multimode acoustic waveguide model, or measured by estimating experimentally the spatial phase gradient in the horizontal plane, $C^{*} = \omega/(\partial\varphi/\partial r)$.

Note that the characteristics of only scalar fields were discussed in [1–5], whereas currently vector-phase (vector-scalar) fields are also of great interest for researchers [6, 7]. In addition, the characteristics of SP field in only the horizontal plane were considered in [3–5] while the dependences on depth z or z_0 were not analyzed.

In what follows, the spatial and frequency amplitude-phase SP characteristics $P(r,\omega,h,z,z_0)$ (referred to as P below) and the horizontal and vertical projections of the SP phase gradient vector and VVV are analyzed for a few-mode waveguide under the following conditions: (a) with variation in the depth of sound source and fixed reception depths and (b) with variation in the depth of receiving antennas and specified (fixed) transmitter depths.

The results obtained are recommended to use in order to increase the detection noise immunity and reduce bearing bias when forming a directional characteristic in shallow water by towed (at different depths) or stationary (for example, bottom) horizontal scalar or vector-scalar antennas, with location of transmitters (noise sources) on different horizons: from the near-bottom region to small depths, typical of above-water sources. The results of our study can also be used to optimize modes of shallow water sensing by vertical transmitting and receiving antennas, forming spatial receiving or transmitting channels in a waveguide.

In view of the well-known practical applications, the vertical field structure in the regions of interference maxima and minima is also of interest for the problems in which a source moves in the vertical direction with a constant velocity at a specified distance from a receiving antenna.

3. THEORETICAL MODELS OF VECTOR-SCALAR FIELD IN A HOMOGENEOUS WAVEGUIDE

Let us consider a point harmonic source, the sound potential of which in an unlimited space has the form $\psi = \psi_0 \exp(-i\omega t)$, where ψ_0 is a factor independent of time t. Under the assumption that the field

is potential, the relationship between the vibration velocity $\overline{V}$ and SP P is given by the well-known formulas [8]: $\overline{V} = \operatorname{grad}\psi$ and $P = -\rho_0(\partial\psi/\partial t) = i\omega\rho_0\psi$, where ρ_0 is the density of the medium.

Let $P = |P|e^{i\varphi} = \mathrm{Re}P + i\mathrm{Im}P$; then, using the above relations, one can show that the orthogonal projections of the SP phase gradient $\operatorname{grad}\varphi$, expressed in terms of the projections of VVV $\overline{V}$, have the form

$$\begin{aligned}\frac{\partial\varphi}{\partial x} &= \frac{\operatorname{Re}V_x\operatorname{Re}P + \operatorname{Im}V_x\operatorname{Im}P}{|P|^2/\omega\rho_0},\\ \frac{\partial\varphi}{\partial y} &= \frac{\operatorname{Re}V_y\operatorname{Re}P + \operatorname{Im}V_y\operatorname{Im}P}{|P|^2/\omega\rho_0},\\ \frac{\partial\varphi}{\partial z} &= \frac{\operatorname{Re}V_z\operatorname{Re}P + \operatorname{Im}V_z\operatorname{Im}P}{|P|^2/\omega\rho_0}.\end{aligned} \tag{3}$$

These relations for different projections of the SP phase gradient can also be derived using the relation $\operatorname{gard}\varphi = (\operatorname{Re}P\times\operatorname{grad}\operatorname{Im}P - \operatorname{Im}P\times\operatorname{grad}\operatorname{Re}P)/|P|^2$ [9].

To determine pressure fields P in a Pekeris waveguide, one can use the well-known integral representation for point-transmitter field potential in the form [8, 10]

$$\psi_0 = A\int\limits_{-\pi/2+i\infty}^{\pi/2-i\infty} H_0^{(1)}(kr\sin\vartheta)\,F(\vartheta)\sin\vartheta\,d\vartheta, \tag{4}$$

where A is the source volume velocity, $H_0^{(1)}(kr\sin\vartheta)$ is a Hankel function, k is the wavenumber, $r = \sqrt{(x-x_0)^2+(y-y_0)^2}$ is the horizontal distance between the transmitter and receiving point,

$$F(\vartheta) = \begin{cases} -\dfrac{[e^{-bh+bz_0}+V_1(\vartheta)\,e^{bh-bz_0}](e^{bz}-e^{-bz})}{e^{-bh}+V_1(\vartheta)\,e^{bh}}, \\ \qquad 0\leqslant z\leqslant z_0; \\ -\dfrac{(e^{bz_0}-e^{-bz_0})[(e^{-bh+bz}+V_1(\vartheta)\,e^{bh-bz}]}{e^{-bh}+V_1(\vartheta)\,e^{bh}}, \\ \qquad z_0\leqslant z\leqslant h, \end{cases} \tag{5}$$

where $b = ik\cos\vartheta$, h is the waveguide thickness, and $V_1(\vartheta)$ is the reflection coefficient from the waveguide bottom.

Integral (4) converges uniformly beyond some arbitrarily small vicinity of the sound source; therefore, the components of VVV $\overline{V}$ can be found by differentiating (4). As a result, we obtain the following expressions for the VVV orthogonal projections of the source under consideration in a Pekeris waveguide:

$$\begin{aligned} V_x &= -\frac{Akx}{r}\int\limits_G H_1^{(1)}(u)\,F(\vartheta)\sin^2\vartheta\,d\vartheta,\\ V_y &= -\frac{Aky}{r}\int\limits_G H_1^{(1)}(u)\,F(\vartheta)\sin^2\vartheta\,d\vartheta,\\ V_z &= -\frac{ikA}{2}\int\limits_G H_0^{(1)}(u)\,F_z(\vartheta)\sin^2\vartheta\,d\vartheta, \end{aligned} \tag{6}$$

where $G = (-\pi/2+i\infty, \pi/2-i\infty)$, $u = kr\sin\vartheta$, and

$$F_z(\vartheta) = \begin{cases} -b\dfrac{[e^{-bh+bz_0}+V_1(\vartheta)\,e^{bh-bz_0}](e^{bz}+e^{-bz})}{e^{-bh}+V_1(\vartheta)\,e^{bh}}, \\ \qquad 0\leqslant z\leqslant z_0; \\ -\dfrac{(e^{bz_0}-e^{-bz_0})[(e^{-bh+bz}-V_1(\vartheta)\,e^{bh-bz}]}{e^{-bh}+V_1(\vartheta)\,e^{bh}}, \\ \qquad z_0\leqslant z\leqslant h. \end{cases} \tag{7}$$

Integrals (4) and (6) can be calculated by direct numerical integration or using the saddle-point method. In addition, applying the technique of residues, one can reduce integrals (6) to sums similar to the sum of normal waves of SP field:

$$\begin{aligned} P &= i\omega\rho_0\sum_{l=0}^{\infty} A_l H_0^{(1)}(r\xi_l),\\ V_x &= -\frac{x}{r}\sum_{l=0}^{\infty} A_l\xi_l H_1^{(1)}(r\xi_l),\\ V_y &= -\frac{y}{r}\sum_{l=0}^{\infty} A_l\xi_l H_1^{(1)}(r\xi_l),\\ V_z &= \sum_{l=0}^{\infty} A_l' H_0^{(1)}(r\xi_l). \end{aligned} \tag{8}$$

Here $u_l = h\sqrt{k^2-\xi_l^2}$; ζ_l $(l = 0,\ 1,\ 2, \ldots)$ are roots of the Pekeris waveguide dispersion equation $\cot x = i\sqrt{x^2-(kh\nu)^2}/mx$, where $m = \rho/\rho_0$ is the ratio of the densities of water and the underlying half-space, $\nu^2 = 1-n^2$, $n = n_0(1+i\widetilde{\alpha})$, $n_0 = c_0/c$ is the ratio of the speeds of sound in the waveguide and soil, $\widetilde{\alpha}$ is the absorption coefficient of the interface; and

$$\begin{aligned} A_l &= -\frac{2\pi u_l\sin\alpha_{l0}\sin\alpha_l}{h(\sin^2 u_l\tan u_l/m^2+\sin u_l\cos u_l - u_l)},\\ A_l' &= u_l\cot\alpha_l/h, \end{aligned} \tag{9}$$

where $\alpha_{l0} = u_l z_0/h$ and $\alpha_l = u_l z/h$.

The calculations presented below were performed using contour integration and an analog of SP field expansion in normal waves, applied to VVV components (see (6) and (8)).

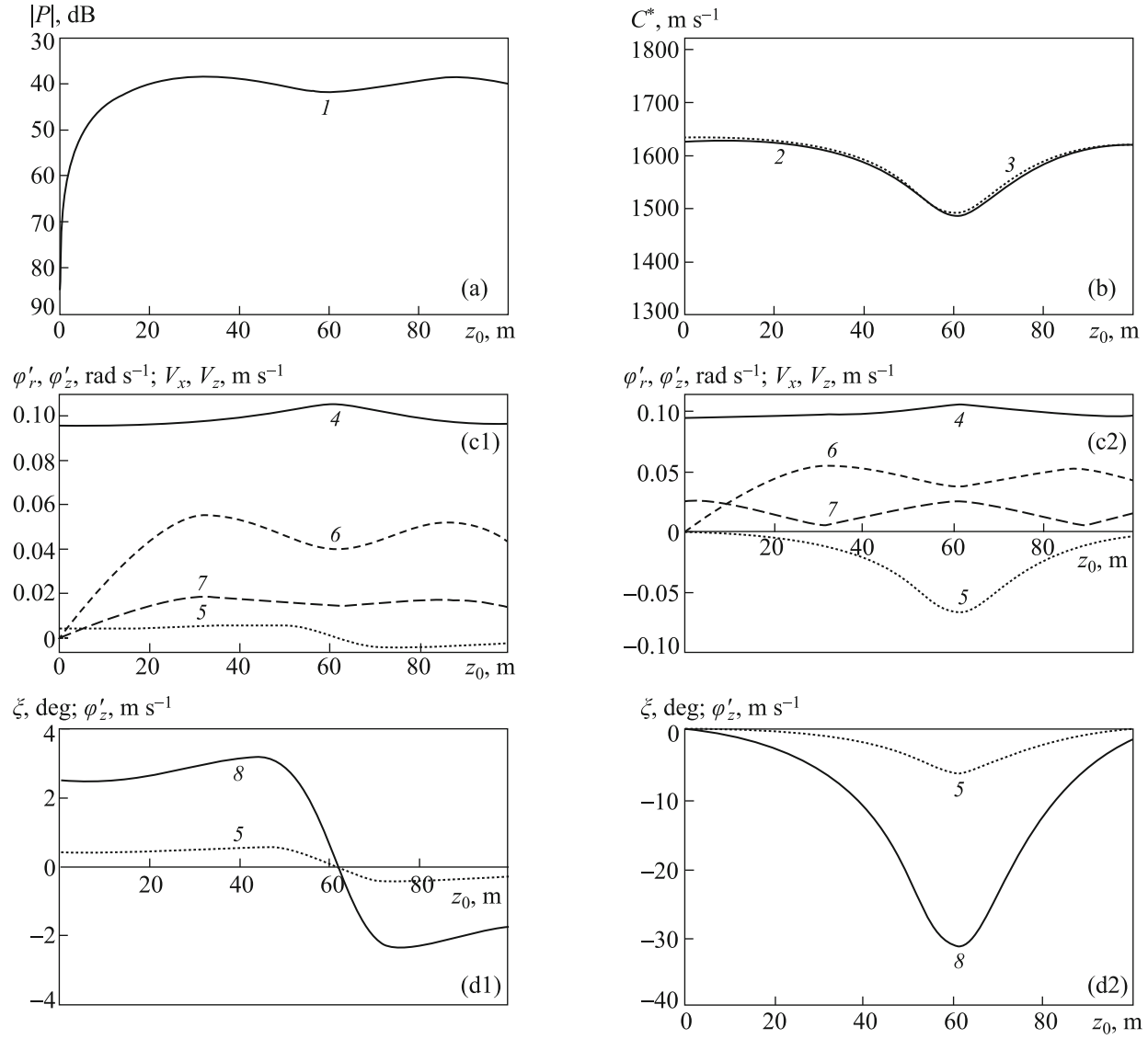

Fig. 1. Amplitude and phase vector-scalar field characteristics for $f = 25$ Hz and $r = 5$ km: dependences on the source depth z_0 at a reception depth $z = 100$ m (on the left) and dependences on the reception depth z at a transmission depth $z_0 = 100$ m (on the right).

4. INITIAL DATA USED IN THE CALCULATIONS

Let us consider the field characteristics for a point source in a Pekeris waveguide, which is a homogeneous water layer of thickness $h = 100$ m, with the speed of sound in water $C_0 = 1450$ m s^{-1}. Calculations will be performed with the following parameters of the bottom: $m = 1.8$, $n = 0.725$, and damping coefficient $\widetilde{\alpha} = 0.02$.

Let the OXY plane of the coordinate system coincide with the waveguide free surface and the OZ axis be directed downwards (to the waveguide bottom).

The following two problems are to be solved. In the first case, a transmitter is located at a depth z_0, which changes from zero (free surface) to h (bottom). The horizontal coordinates of the transmitter are assumed to be zero: $x_0 = 0$ and $y_0 = 0$. A four-component vector-scalar acoustic receiver (or multielement antenna) is located in the horizontal plane at a distance $x = 5$ or 20 km from the transmitter. The receiver depths are $z = 50$ and 100 m. We assume that $y = 0$ and $r = x$ because $r \gg h$.

In the second case, a vector-scalar receiving antenna is located at a depth z, which changes from zero (free surface) to h (bottom). The horizontal coordinates of four-component receivers are assumed to be zero: $x_0 = 0$ and $y_0 = 0$. The transmitter (or transmitting antenna) is located in the horizontal plane at a distance $x = 5$ or 20 km from the receiving antenna. The transmitter depths are $z_0 = 50$ and 100 m. We assume, as above, that $y = 0$ and $r = x$ because $r \gg h$.

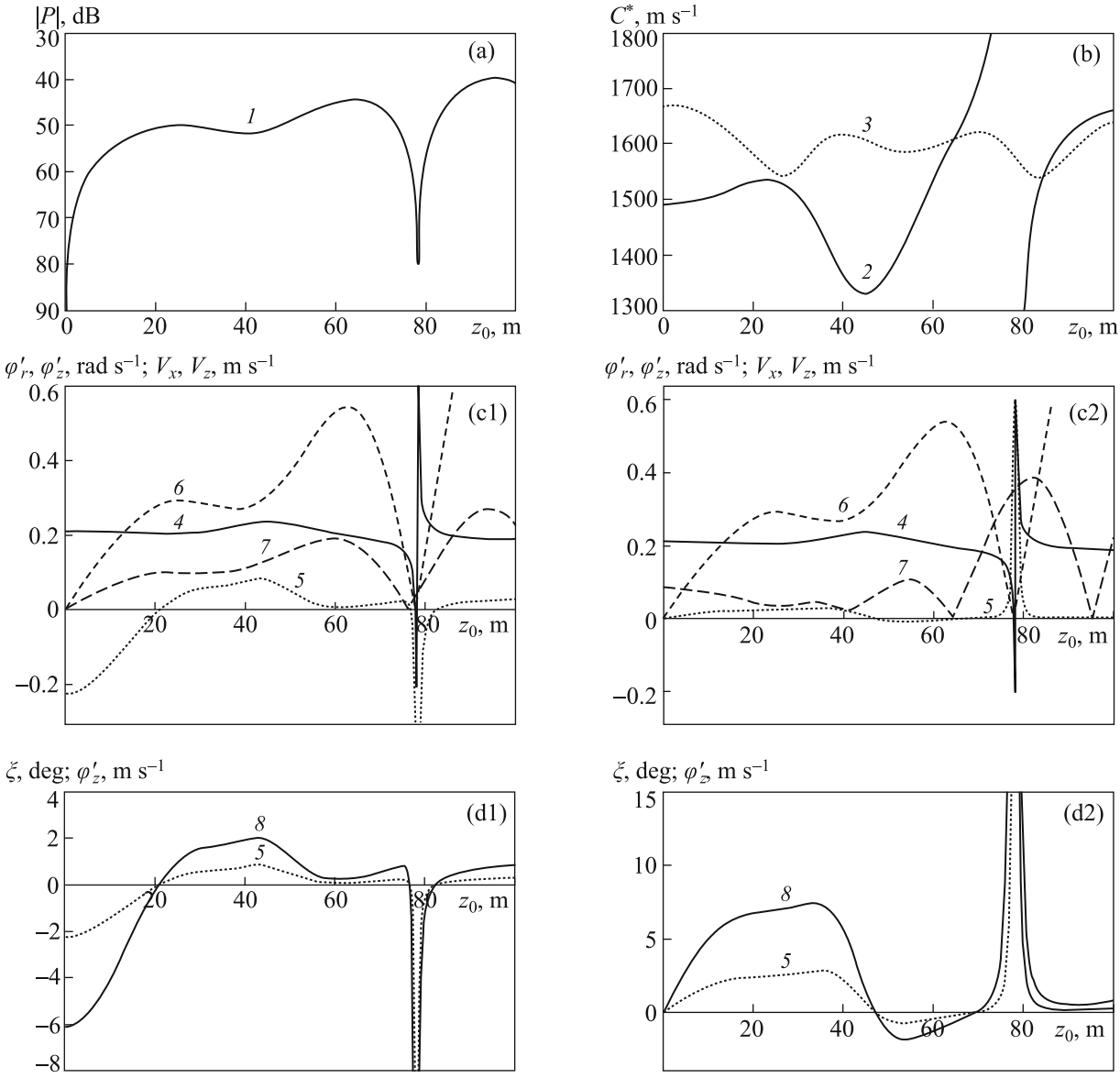

Fig. 2. Amplitude and phase vector-scalar field characteristics under the same conditions as in Fig. 1 but for a frequency $f = 50$ Hz.

Let us investigate the amplitude and phase vector-scalar field characteristics in a waveguide for the purposes of solving the problems of weak-signal detection and direction finding against the noise background. To this end, we will analyze the field structure in the regions of interference maxima and minima ($P_{\max}$ and $P_{\min}$). Then in contrast to [4, 5], the emphasis is on the dependences of the field characteristics on the variables z and z_0. In the $P_{\max}$ and $P_{\min}$ regions, we investigate also the dependences of the effective phase velocity (which characterizes local phase gradients in the horizontal plane) on the reception or transmission depth at fixed frequencies.

The field characteristics obtained using different schemes of computational experiment are compared in Figs. 1–8. The field characteristics as functions of the source depth z_0 at two fixed reception depths, $z = 50$ and 100 m, are shown on the left, and the characteristics as functions of the reception depth z at two fixed source depths, $z_0 = 50$ and 100 m, are presented on the right.

The curves in Figs. 1–8 are enumerated as follows: (*1*) (plots (a)) SP amplitude $|P|$; (*2*) (b) effective phase velocity C^* calculated from the SP phase gradient; (*3*) (b) effective phase velocity C^* calculated from approximate formula (1); (*4*) (c1, c2) longitudinal component of the phase gradient, $\varphi'_r = \partial\varphi/\partial r$; (*5*) (c1, c2, d1, d2) vertical component of the phase gradient, $\varphi'_z = \partial\varphi/\partial z$; (*6*) (c1, c2) amplitude of the VVV horizontal component V_x; (*7*) (c1, c2) amplitude

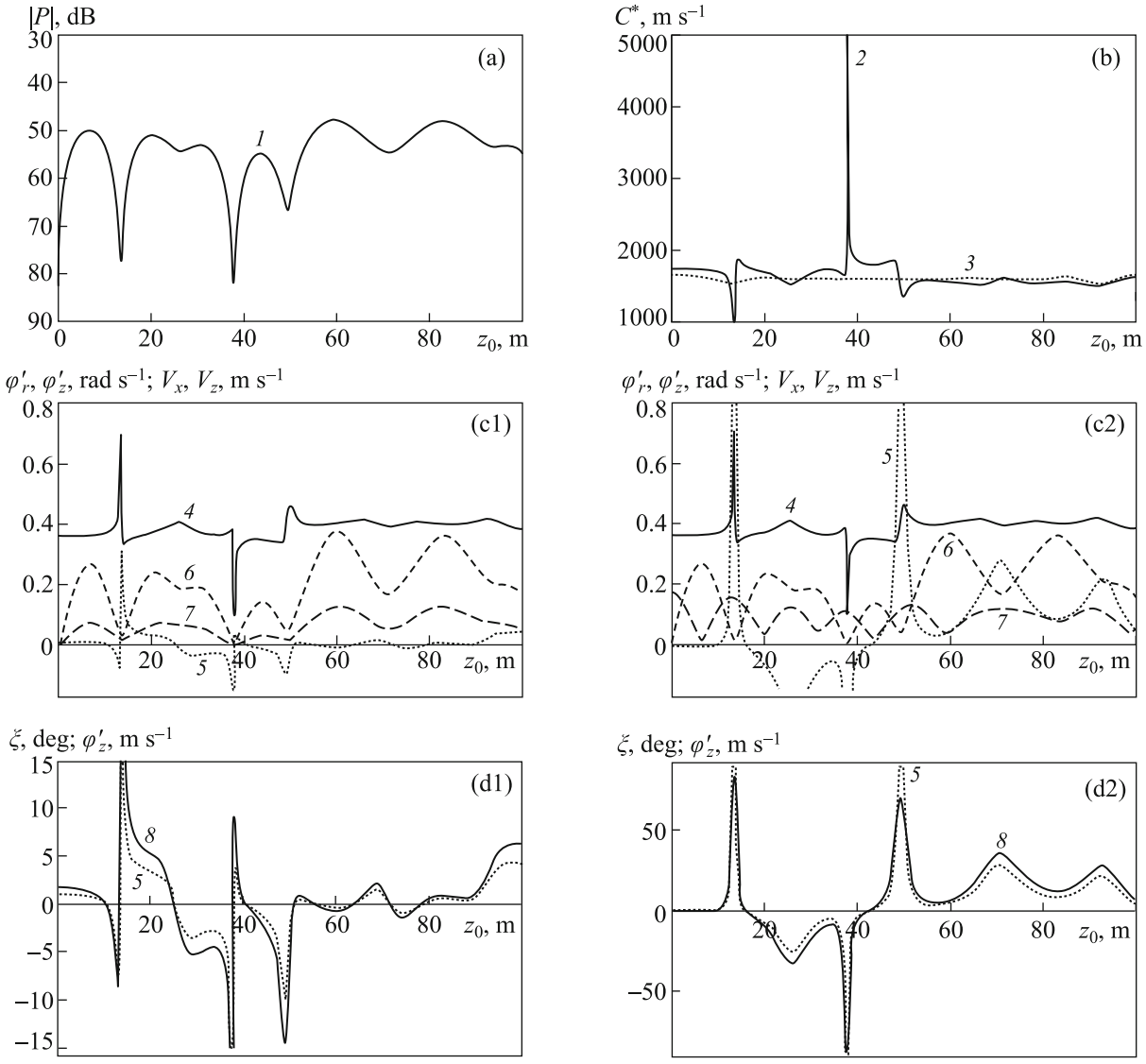

Fig. 3. Amplitude and phase vector-scalar field characteristics under the same conditions as in Fig. 1 but for a frequency $f = 100$ Hz.

of the VVV vertical component V_z; and (*8*) (d1, d2) directional angle of phase gradient ξ (EPW arrival angle) in polar coordinates in the vertical cross section of the sound field. The VVV components in plots (c1) and (c2) are scaled with a factor of 5 or 100, while the VVV and phase gradient components in plots (d1) and (d2) are scaled with a factor of 100.

Calculations showed that the dependences of the SP amplitudes $P(z)$ and $P(z_0)$ (curve *1*), the effective phase velocities $C^*(z)$ and $C^*(z_0)$ (curves *2* and *3*, calculated from different formulas), the horizontal projections of the SP phase gradient $\varphi'_r = \partial\varphi(z)/\partial r = \partial\varphi(z_0)/\partial r$ (curves *4*), and the VVV horizontal projection $V_r(z, z_0)$ (curves *6*) on the transmission or reception depths, as one would expect, turned out to be identical for the two above-stated problems. In this context, they are shown for only one case. This circumstance indicates that the reciprocity principle is satisfied for scalar fields and horizontal components of vibration velocity in the waveguide.

The dependences of the vertical components of the SP phase gradient, $\partial\varphi(z)/\partial z$ and $\partial\varphi(z_0)/\partial z$ (curves *5*), the vertical VVV projections $V_z(z)$ and $V_z(z_0)$ (curves *7*), and the phase gradient direction (i.e., the EPW arrival angle, equal to the grazing angle of the SP phase gradient) (curves *8*) on depths z and z_0 are significantly different; they are presented in the figures on the right and on the left, respectively.

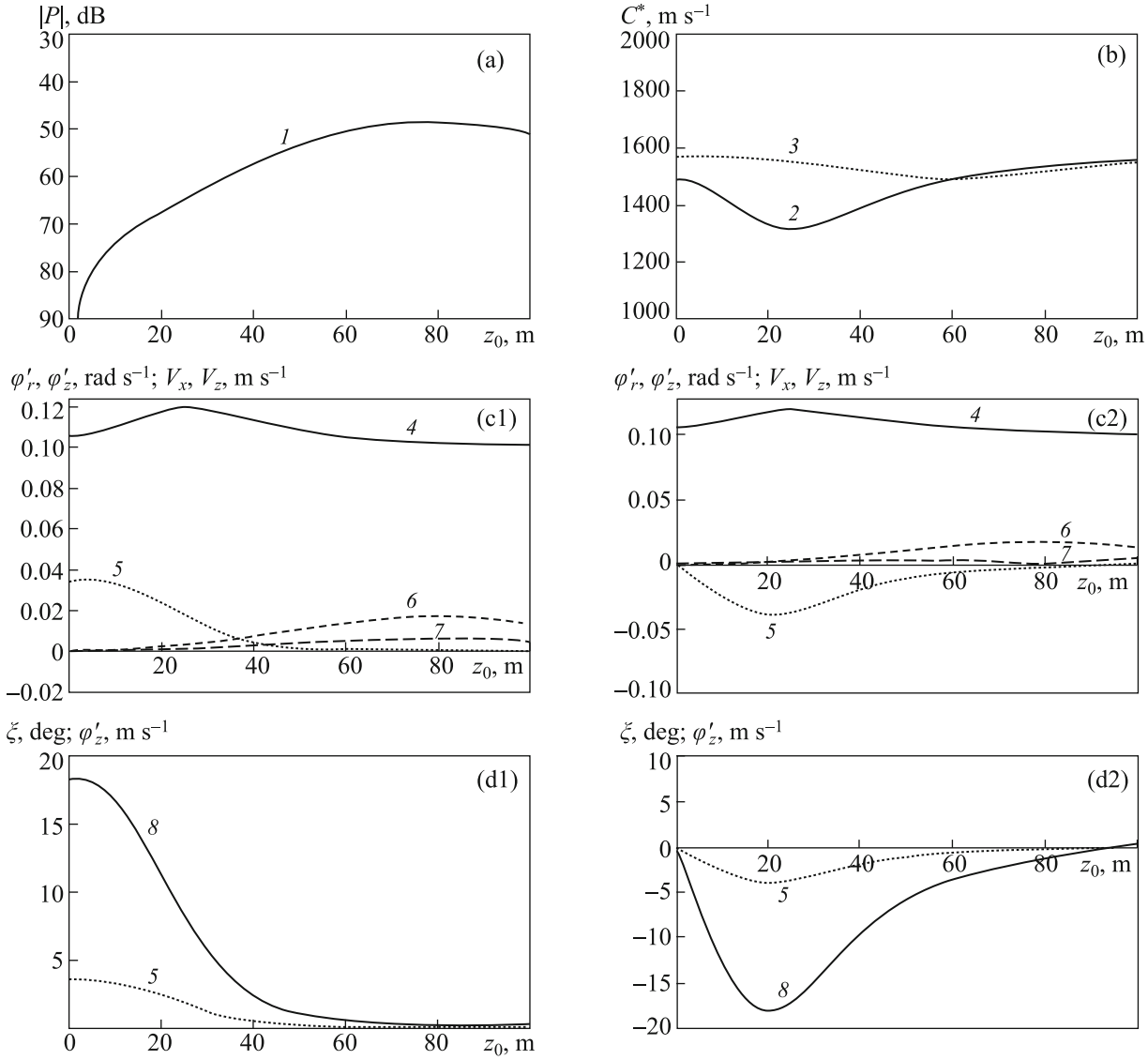

Fig. 4. Amplitude and phase vector-scalar field characteristics under the same conditions as in Fig. 1 but for a distance $r = 20$ km.

5. RESULTS OF NUMERICAL ANALYSIS OF THE AMPLITUDE AND PHASE INTERFERENCE STRUCTURE OF VECTOR-SCALAR FIELD

Figures 1–4 show the calculation results for different frequencies of transmitted harmonic signal and two distances (5 and 20 km), which were obtained on the assumption that transmission or reception occur in the near-bottom region ($z = 0$ or $z_0 = 0$) and that the transmitter or receiving antenna depths change in the range from 0 to h.

According to the results presented in Fig. 1, the specified conditions and two-mode field model provide fairly uniform filling the waveguide, with a small interference minimum at the depth corresponding to the effective-waveguide middle, $h^* = h + \Delta h \approx 124.4$ m [11]. Correspondingly, only small inhomogeneities of phase gradient $\varphi'_r = \partial\varphi(z)/\partial r = \partial\varphi(z_0)/\partial r$ are observed; as a consequence, the C^* values calculated both from the analytical dependence (via modes) and directly (using the SP phase gradient) almost coincide and change only slightly with z or z_0.

In the $P_{\max}$ region, the C^* value greatly exceeds C_0, whereas $C^* \to C_0$ in the $P_{\min}$ region.

Note that the dependences of amplitudes P or V_r on z or z_0 are similar. The dependence $V_z(z_0)$ for reception in the near-bottom region is also similar to the dependences $P(z, z_0)$ and $V_r(z, z_0)$. At the same time, the behavior of $V_z(z)$ is almost in antiphase with that of $V_z(z_0)$ that is in exact correspondence with theoretical relations (8) and (9), according to which the normal-wave amplitude $V_z(z)$ is propor-

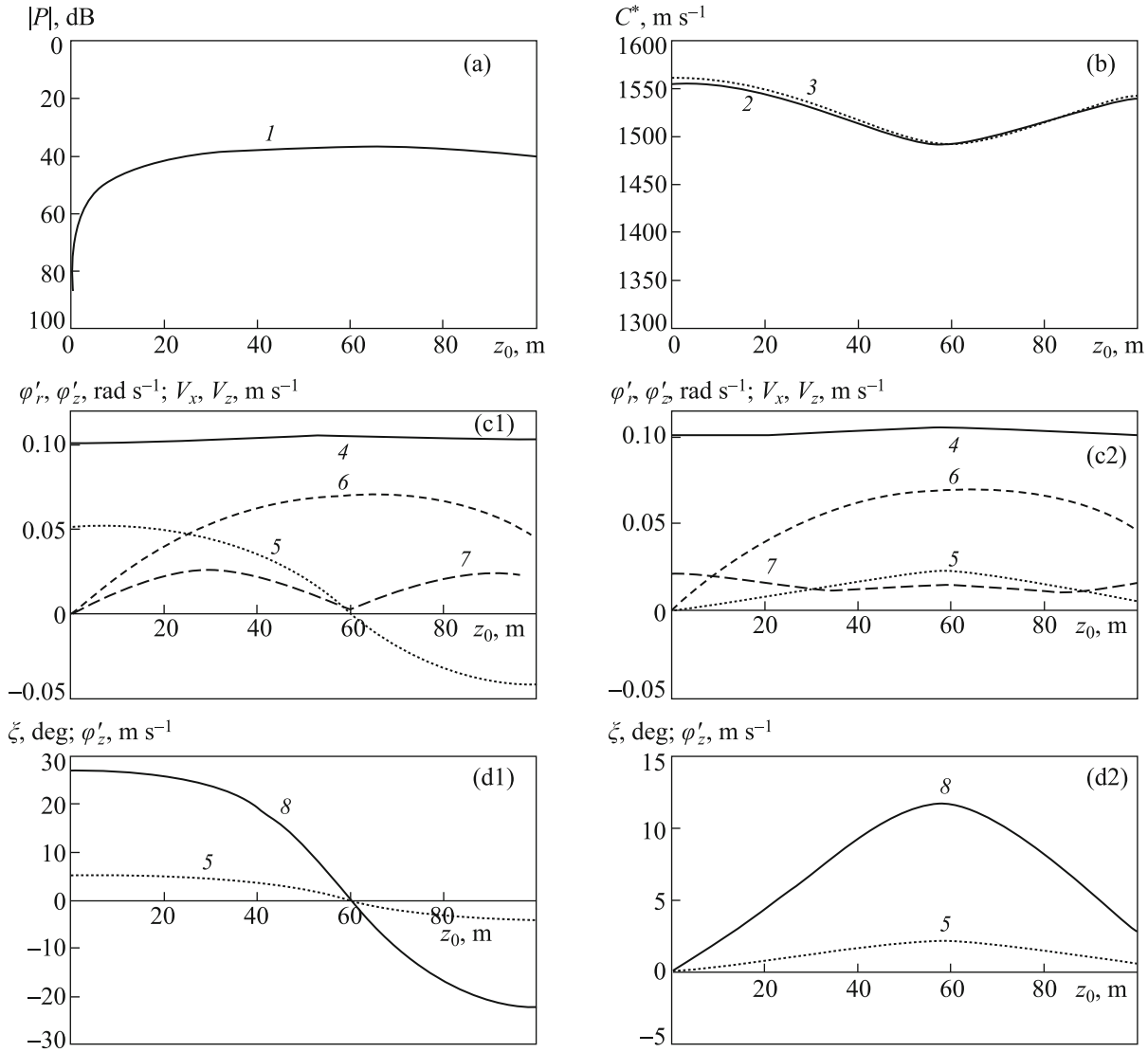

Fig. 5. Amplitude and phase vector-scalar field characteristics for $f = 25$ Hz and $r = 5$ km: dependences on the source depth z_0 at a reception depth $z = 50$ m (on the left) and dependences on the reception depth z at a transmission depth $z_0 = 50$ m (on the right).

tional to $\cos z$ while the normal-wave amplitude is proportional to $V_z(z_0) \to \sin z_0$.

There is a fundamental difference in the dependences $\varphi'_{z_0} = \partial\varphi(z_0)/\partial z_0$ (curve *5* on the left) and $\varphi'_z = \partial\varphi(z)/\partial z$ (curve *5* on the right) for these two versions. Since variations in φ'_r are small, a difference in φ'_z and φ'_{z_0} leads also to a radical difference in the dependences of EPW arrival angles (grazing angles of the SP phase gradient) on z or z_0: the $\xi(z_0)$ plot contains an inflection at the point corresponding to $P_{\min}$, which separates the regions of EPW arrival at the receiving point from above or below, and $\zeta(z)$ has a deep minimum in the $P_{\min}$ region.

A significant difference is observed for the dependences $V_z(z)$ and $V_z(z_0)$. The $P(z_0)$, $V_r(z_0)$, and $V_z(z_0)$ values also decrease monotonically and tend to zero with a decrease in z_0 ($z_0 \to 0$). This is quite natural because the transmitter near the free surface has a zero transmission resistance due to the Lloyd effect.

At $z \to 0$, $V_z(z)$ takes rather large values. This conclusion is in complete agreement with the cosine dependence of the expansion coefficients $V_z(z)$ on z and with the results of classical analysis of the behavior of differently oriented dipoles near soft and rigid surfaces. It was shown in [12, 13] that the pressure amplitudes for horizontal dipoles near a free surface (at $kz < 1$, where $k = \omega/C_0$), as well as the monopole pressure, tend to zero while vertical dipoles double the amplitude. On the contrary, the amplitude $V_z(z)$

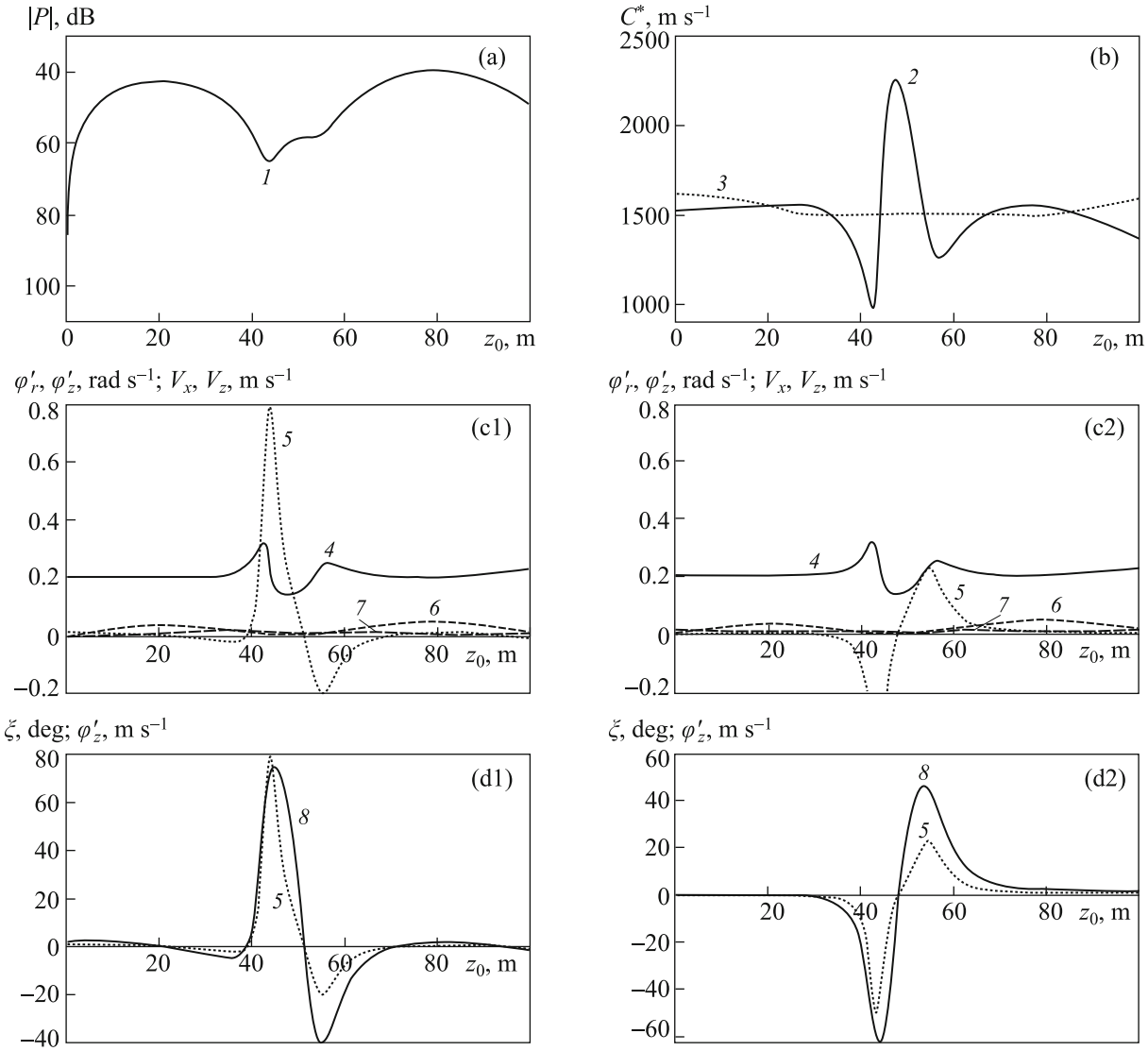

Fig. 6. Amplitude and phase vector-scalar field characteristics under the same conditions as in Fig. 5 but for a frequency $f = 50$ Hz.

near bottom should decrease at $k(h - z) < 1$, which is observed in Figs. 1–4 (curves *6*).

At the same time, $z \to h$ at z_0, i.e., when a transmitter or a scalar receiving element is located near the bottom, the amplitude of the signal transmitted by monopole, as well as the received values of sound pressure or VVV horizontal projections should increase. This conclusion is confirmed by the data in Fig. 1(c1, c2).

Figure 2 presents data similar to those in Fig. 1 but for a frequency of 50 Hz.

It can be seen that the region of deep minimum ($P_{\min}$) exhibits large deviations of horizontal projections of the SP phase gradient and, correspondingly, C^* from mean values. In this case, the C^* value is stabilized in the $P_{\max}$ region, but the inequality $C^* > C_0$ is retained.

Note that the region of deep minimum ($P_{\min}$) is characterized by alternating jumps of $\varphi'_r(z, z_0)$ (close to break of continuity), which indicates proximity of dislocation [9, 14, 15]. The change in the phase gradient sign along the current line confirms the formation of reverse energy flux, i.e., the occurrence of vorticity.

The other calculation results are similar to those presented in Fig. 1. Specifically, the dependences $P(z_0)$, $V_r(z_0)$, and $V_z(z_0)$ are similar for near-bottom reception; the dependences $P(z)$ or $V_r(z)$ are similar and in antiphase with $V_z(z)$; the functions $P(z_0)$, $V_r(z_0)$, and $V_z(z_0)$ tend to zero at $z_0 \to 0$; and the dependences $P(z)$ or $V_r(z)$ also tend to zero at $z \to 0$, whereas $V_z(z)$ becomes nonzero at $z \to 0$.

As in Fig. 1, one can see a significant difference between the dependences $\varphi'_z(z)$ and $\varphi'_z(z_0)$, as well as

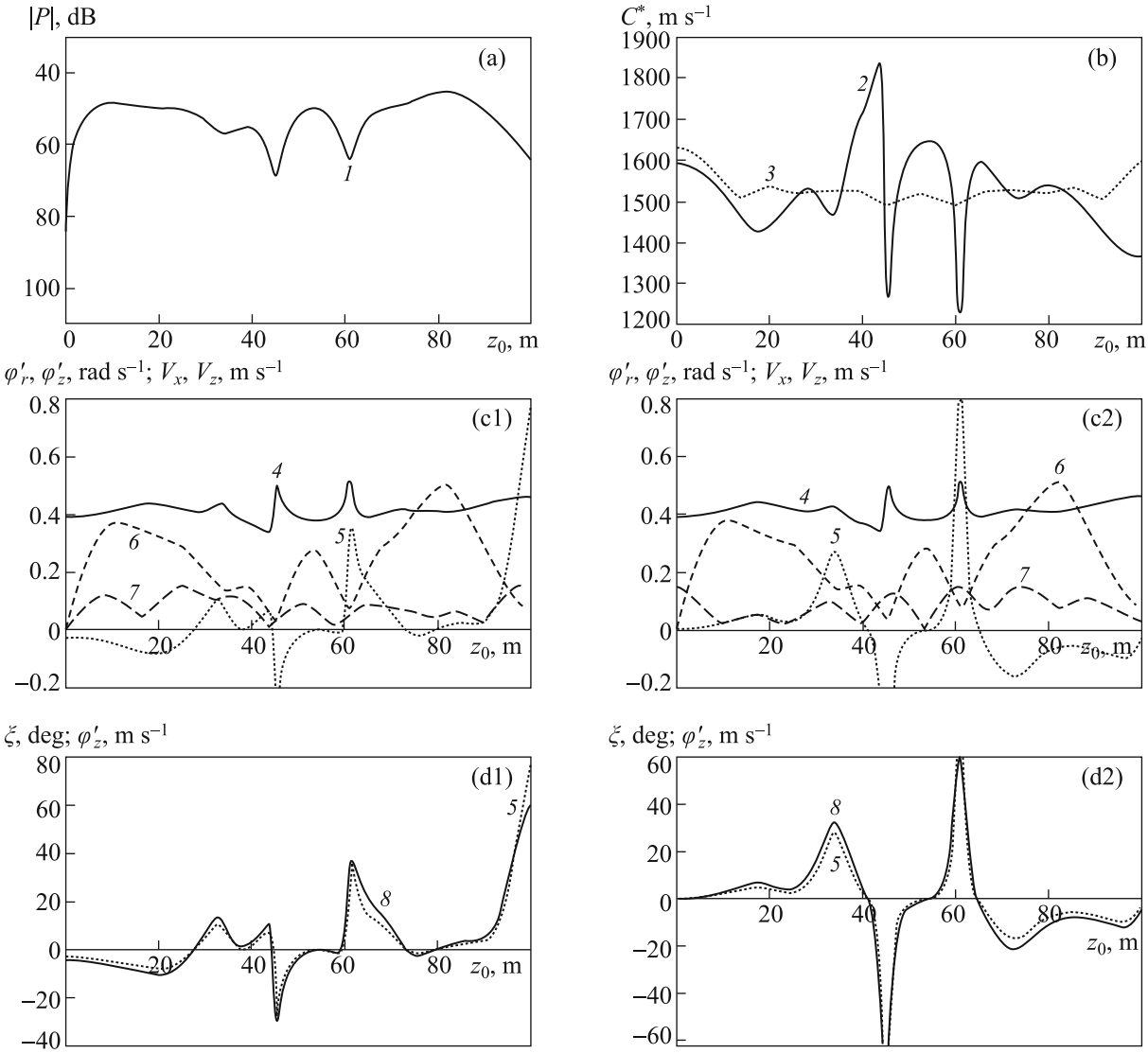

Fig. 7. Amplitude and phase vector-scalar field characteristics under the same conditions as in Fig. 5 but for a frequency $f = 100$ Hz.

between the EPW arrival angles at the receiving point $\xi(z, z_0)$: these values change almost in antiphase with variation in z or z_0.

Figure 3 corresponds to even higher frequency (100 Hz). The number of extreme regions ($P_{\max}$ or $P_{\min}$) is larger in this case. The reason is that the occurrence of modes with large numbers leads to an increase in the intervals between the wave numbers, thus narrowing the $P_{\max}$ regions and, correspondingly, increasing the number of these regions.

It can be seen that, as in Fig. 2, the deep $P_{\min}$ region exhibits jumps of phase gradients, both $\varphi'_r(z, z_0)$ and $\varphi'_z(z, z_0)$. Unrealistically large (or small) C^* values correspond to these regions, and large alternating deviations of the EPW arrival angle from horizontal arise. At the same time, the deviations of angle ξ in $P_{\max}$ regions are small, and the ξ value is close to constant within large intervals Δz or Δz_0 that allows one to form efficiently spatial channels in these intervals (directional characteristics) using vertical receiving or transmitting antennas.

Figure 4 shows the calculation results for the conditions similar to those illustrated in Fig. 1 but for a much larger distance to the transmitter: 20 km. It can be seen that its amplitude and the first-mode amplitude become comparable at a smaller depth z or z_0 in comparison with Fig. 1 because of the stronger damping of the second mode. As a consequence, all curves are on the whole distorted, and anomalous portions with singularities shift to smaller z or z_0 values. Other characteristic regularities are similar to those described above.

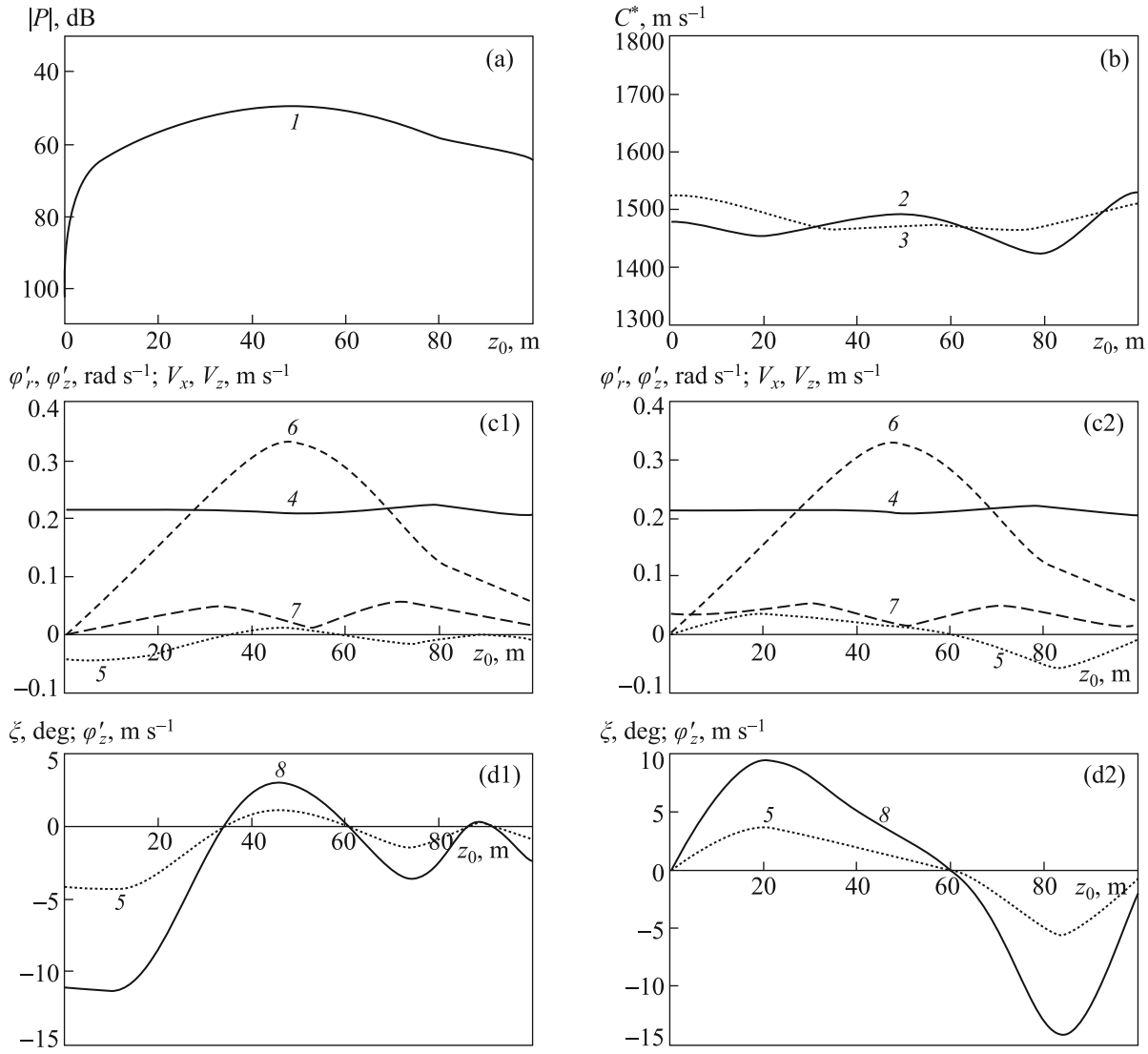

Fig. 8. Amplitude and phase vector-scalar field characteristics under the same conditions as in Fig. 5 but for a frequency $f = 50$ Hz and distance $r = 20$ km.

Similar calculation results were obtained for other frequencies (50, 100, and 200 Hz), all other factors being equal. On the whole, an increase in the distance reduces the contribution of modes with large numbers and decreases the number of anomalous (extreme) regions, while the dependences $C^*(z, z_0)$ are smoothed out.

Figures 5–8 show the calculation results obtained on the assumption that signal reception (with variation in the source depth z_0) or transmission (with variation in the receiver depth z) is performed at a depth of 50 m (almost in the middle of the effective waveguide). Figures 5–7 were obtained at a distance of 5 km to the transmitter; the distance for Fig. 8 is 20 km.

It follows from Figs. 5–7 that, when a receiving antenna or transmitter are located in the middle of the waveguide, the interference is smoothed out in comparison with the near-bottom region, which corresponds to the experimental data of [16] and the results of computer simulation [17]. The characteristics $P(z, z_0)$, $V_r(z, z_0)$, and $\varphi'_r(z, z_0)$ are qualitatively the same as for the near-bottom reception. However, the dependences $V_z(z)$ and $V_z(z_0)$ in the case of reception (or transmission) in the middle of the waveguide are in antiphase with the dependences $P(z, z_0)$ and $V_r(z, z_0)$.

It can also be seen that, as for the near-bottom reception (transmission), the $P_{\min}$ region contains anomalous zones, characterized by a change in the signs of $\varphi'_r(z, z_0)$ and $\varphi'_z(z, z_0)$. This fact indicates formation of singularities (dislocations). As was shown in [9, 14, 15], a saddle-like phase front should be formed near dislocations in the zones with a

change in the sign of gradients, i.e., at zero values of $\varphi'_r(z, z_0)$ and $\varphi'_z(z, z_0)$.

On the whole, the character of the dependences of scalar or vector field on z and z_0 obeys general regularities; at the same time, anomalous zones manifest themselves (primarily, in the $P_{\min}$ regions).

Figure 8 shows the calculation results for the same conditions as in Fig. 6 for the distance which is now 20 km. It can be seen that, in the regions of interference maxima, the effective phase velocity C^* is almost constant and changes in antiphase with a change in the longitudinal SP phase gradient. It can also be seen that V_r and V_z also change in antiphase, and that $V_z(z)$, in contrast to $P(z, z_0)$ and $V_r(z, z_0)$, tends to a constant (nonzero) value at $z \to 0$.

Note that, as in Fig. 6, the SP phase gradient in the vertical plane and the EPW arrival angles at the receiving point change with a variation in z or z_0 with respect to the horizontal plane (mainly in opposite directions).

6. CONCLUSIONS

We theoretically investigated the spatial sound pressure structure, horizontal and vertical projections of the vibration velocity vector, orthogonal projections of the SP phase gradient, and the EPW arrival angles at a receiving point with a variation in the transmitter depth (reception in the middle of the waveguide and in the near-bottom region) and with a variation in the receiver depth (transmission in the middle of the waveguide and in the near-bottom region).

Analytical relations were obtained to describe the vector-scalar field in shallow water, and calculations were performed using contour integration and an analog of SP field expansion in normal waves, applied to the VVV orthogonal components.

It was established that the characteristics of the scalar field, the VVV horizontal projection, and the SP phase gradients in the horizontal plane satisfy the reciprocity principle: identical characteristics are obtained by recalculating the aforementioned parameters from the transmission point to the receiving point or vice versa. For the vertical components of VVV or SP phase gradient, the reciprocity condition is not fulfilled. As a consequence, one cannot obtain identical EPW arrival angles at the receiving point. Thus, the vertical projections $V_z(z, z_0)$ and $\varphi'_z(z, z_0)$ must be studied separately from the characteristics $\xi(z, z_0)$.

It was shown that the effective phase velocity C^* in $P_{\max}$ regions slowly changes with variation in z or z_0, always exceeds the speed of sound in water C_0 by 5 to 15%, and can be calculated both using the analytical dependence (via the normal-wave characteristics) and through direct calculation of the phase gradient (experimentally or by simulation). It was recommended to use the C^* value instead of C_0 to form a directional characteristic, obtain unbiased bearing estimates, and increase the detection noise immunity.

The behavior of the dependences $P(z, z_0)$ and $V_r(z, z_0)$ with a change in z or z_0 is mutually similar, and the dependence $V_z(z, z_0)$ can be either in phase with these characteristics (case of near-bottom reception) or in antiphase (if reception or transmission are performed in the middle of the waveguide).

The behavior of the dependences $V_r(z, z_0)$ and $V_z(z, z_0)$ and projections $\varphi'_r(z, z_0)$ and $\varphi'_z(z, z_0)$ is consistent well with the pattern of interference maxima and minima: smooth dependences are observed in $P_{\max}$ regions and singularities (dislocation and saddle-type points) are formed in regions with deep $P_{\min}$; these points are characterized by a change in the gradient signs, indicative of the formation of backward energy flux and vorticity.

When z or z_0 tend to zero, the $P(z_0)$, $V_r(z_0)$, and $V_z(z_0)$ values decrease and tend to zero whereas $V_z(z)$ reaches a nonzero value that is in good correspondence with the general theoretical concepts.

When receivers (transmitters) are located in the near-bottom region, the interference field is brighter than for their location in the middle of the waveguide.

The above results suggest that, depending on the specific conditions of signal transmission and reception, there is a large variety of vector-scalar field characteristics. To use efficiently vector-scalar antennas or vector-scalar modules, one must take into account a much larger set of hydroacoustic field characteristics in a waveguide than in the case of scalar fields. However, the use of this approach increases simultaneously the amount of processed data and should improve the detection noise immunity and accuracy in describing the characteristics of weak signals against the noise background.

The use of vector-scalar (four-dimensional) hydroacoustic field characteristics should facilitate gaining a deeper insight into the hydrophysical characteristics of fields in shallow or deep water.

REFERENCES

1. A.B. Baggeroer and W.A. Kuperman, "Matched Field Processing in Ocean Acoustics," in *Acoustic Signal Processing for Ocean Exploration*. Ed. by J.M.F. Moura and I.M.G. Lourtie (Kluwer Academic Publishers, Dordrecht, Boston, London, 1992), pp. 79–114.
2. B.G. Katsnel'son and V.G. Petnikov, *Shallow Water Acoustics* (Nauka, Moscow, 1997) [in Russian].

3. G.A. Grachev and G.N. Kuznetsov, "On the Average Rate for Phase Variation in the Acoustic Field along the Flat Waveguide," Sov. Phys.-Acoust. **31**(2), 266 (1985) [in Russian].
4. G.N. Kuznetsov and O.V. Lebedev, "The Possibility of Using the Equivalent Plane Wave Model to Increase the Efficiency of Taking Bearings of Low-Frequency Signals in Shallow Water," Acoust. Phys. **58**(5), 575 (2012).
5. G.N. Kuznetsov and O.V. Lebedev, "Bearing Determination of Low-Frequency Sources in a Wave Guide by Sonar Systems with Towed or Hull Antennas, " Gidroakustika. **17**(1) (2013) [in Russian].
6. V.A. Shchurov, *Vector Acoustics of the Ocean* (Dal'nauka, Vladivostok, 2003) [in Russian].
7. V.A. Gordienko, *Vector-Phase Methods in Acoustics* (Fizmatlit, Moscow, 2007) [in Russian].
8. L.M. Brekhovskikh, *Waves in Layered Media* (Academic Press, N.Y., 1980).
9. V.A. Zhuravlev, I.K. Kobozev, and Yu.A. Kravtsov, "Detecting Dislocations by Measuring the Energy Flux of an Acoustic Field," JETP. **77**(5), 808 (1993).
10. A.N. Stepanov, *Multipole Model of Hydroacoustic Sources* (Izd-vo Samar. Univ., Samara, 2000) [in Russian].
11. D.E. Weston, "A Moire Fringe Analog of Sound Propagation in Shallow Water," J. Acoust. Soc. Am. **65**(2), 647 (1960).
12. E. Skuchik, *The Foundations of Acoustics* (Springer, N.Y., 1971).
13. M.Ya. Isakovich, *General Acoustics* (Nauka, Moscow, 1973) [in Russian].
14. V.A. Eliseevnin and Yu.I. Tuzhilkin, "Acoustic Power Flux in a Waveguide," Acoust. Phys. **47**(6), 688 (2001).
15. V.M. Kuz'kin, A.V. Ogurtsov, and V.G. Petnikov, "The Effect of Hydrodynamic Variability on Frequency Shifts of the Interference Pattern of a Sound Field in a Shallow Sea," Acoust. Phys. **44**(1), 77 (1998).
16. A.I. Belov and G.N. Kuznetsov, "Characteristics of Normal Waves Exited by Vertical Arrays in Shallow Sea," Phys. Wave Phenom. **14**(3), 66 (2006).
17. G.N. Kuznetsov and A.N. Stepanov, "The Field of an Equivalent Multipole Composite Radiator in a Waveguid," Acoust. Phys. **53**(3), 326 (2007).